analytical chemistry

pubs.acs.org/ac Article

Enhancing Ion Signals and Improving Matrix Selection in Time-of-Flight Secondary Ion Mass Spectrometry with Microvolume Expansion Using Large Argon Clusters

Benjamin Tomasetti, Clément Lauzin, and Arnaud Delcorte*

Cite This: *Anal. Chem.* 2023, 95, 13620−13628 Read Online

ACCESS | Metrics & More | Article Recommendations | Supporting Information

ABSTRACT: The molecular environment has an important impact on the ionization mechanism in time-of-flight secondary ion mass spectrometry (ToF-SIMS). In complex samples, desorption/ionization, and thus the detection of a molecular signal, can be hampered by molecular entanglement, ionization-suppressive neighbors, or even an unfavorable sample substrate. Here, a method called microvolume expansion is developed to overcome these negative effects. Large argon clusters are able to transfer biomolecules from a target to a collector in vacuum. In this study, argon gas cluster ion beams (Ar_n^+-GCIB with n centered around 3000 or 5000) are used to expand a microvolume from the sample to a collector, which is a material ideally enhancing the ionization yield. The collector is then analyzed using a liquid metal ion gun. The signal amplification factor corresponding to the expansion of phosphatidylcholine (PC) lipid on collectors partially covered with acidic matrices was evaluated as an initial proof of concept. In one experiment, the PC expansion on a pattern of four drop-casted matrix-assisted laser desorption/ionization matrices led to the selection of α-cyano-4-hydroxycinnamic (CHCA) as the optimal candidate for cationic PC detection. The ion signal is increased by at least three orders of magnitude when PC was expanded using 10 keV Ar_{3000}^+ and Ar_{5000}^+ on a sublimated layer of CHCA. Finally, the expansion of the gray matter of a mouse on different materials (Si, Au-coated Si, CHCA, and polyethylene) was achieved with varying degrees of success, demonstrating the potential of the method to further analyze complex and fragile biological assemblies.

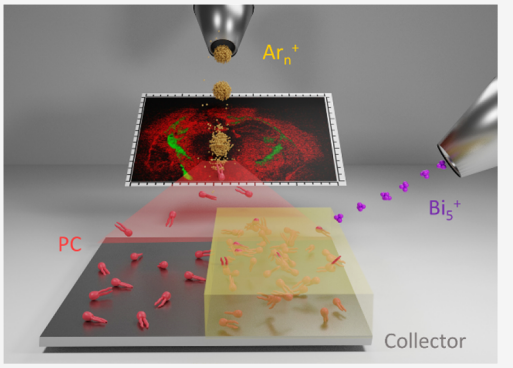

INTRODUCTION

Due to its high resolution and its 2D and 3D molecular imaging capabilities, time-of-flight secondary ion mass spectrometry (ToF-SIMS) is an increasingly popular method in metabolic studies.[1,2] However, analysis of such chemically complex materials is not straightforward. There are complications in achieving a true spatial resolution of 100 nm for molecular analysis. Indeed, if liquid metal ion gun (LMIG) sources can be highly focused, their primary ions fragment the molecules and create subsurface damage. Therefore, when performing surface analysis, it is desirable to remain below the so-called static SIMS limit, for which the probability that an incident ion hits an already damaged area remains negligible. To avoid a subsequent decrease in the molecular secondary ion yield, it is generally admitted that the primary ion dose must be kept below 10^{12} to 10^{13} ions/cm^2.[3] Therefore, adding to this the low ionization probability, the creation of a sufficient number of molecular ions from a reduced pixel size becomes very challenging or even impossible in many cases.

However, the static limit is much less of a concern for large clusters such as C_{60}^+ or Ar_n^+ within certain limits of sample type and/or energy.[4] Indeed, it was shown that the higher sputter yield and the lower penetration depth of these cluster ions lead to a strong reduction of damage. That is why the Ar_n^+-GCIB was first used to remove the damage created by the LMIG.[5] This dual beam method allows to overcome the static limit as the damage is removed between LMIG beam analyses. However, 95% of the material is sputtered without being analyzed.

More recently, GCIB have gained popularity as primary ion sources for analysis. If the mass resolution was already increased by delayed extraction,[6] significant advances in SIMS instrumentation enabled simultaneous high mass resolving power and subcellular spatial resolution with large clusters. Such instruments include a quadrupole orthogonal time-of-flight (ToF) spectrometer for the J105 (IONOPTIKA, UK) instrument[1] and a Q exactive HF Orbitrap for the 3D OrbiSIMS instrument.[7] The J105 instrument allows a continuous primary ion beam to be used for analysis because the beam bunching and pulsing are performed in the harmonic reflectron mass analyzer, with a large

Received: June 2, 2023
Accepted: August 9, 2023
Published: August 23, 2023

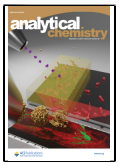

https://doi.org/10.1021/acs.analchem.3c02404
Anal. Chem. 2023, 95, 13620−13628

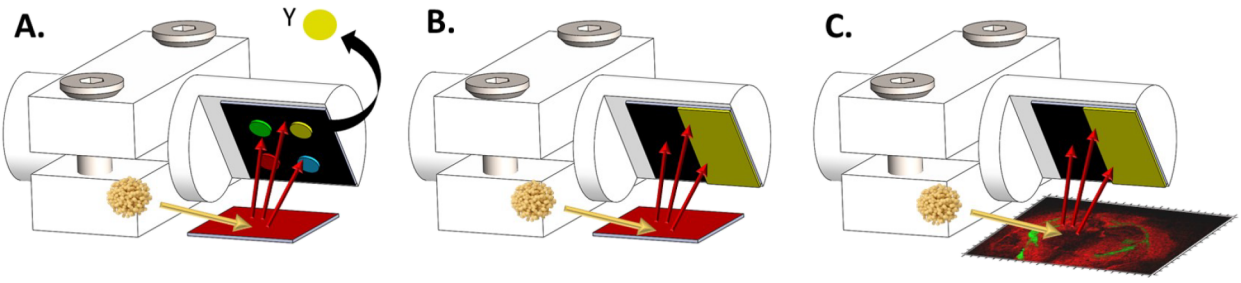

Figure 1. Chronology of experiments exploiting the concept of microvolume expansion for the detection of a target molecule. In each case, only the transfer procedure is illustrated and is followed by an analysis using a Bi_5^+ beam. (A) A reference sample is transferred on a pattern of matrices. The best matrix is selected based on properties such as secondary ion yield, *Y*. (B) The reference sample is transferred on a collector with the best sublimated matrix on one half. (C) The matrix is used for the detection of the molecule on a real tissue.

fraction of the secondary ions being retained. The duty cycle and the resulting acquisition rate are greatly increased with respect to conventional ToF instruments and depth profiles can be performed with a maximized sensitivity since a large part of the valuable material sputtered by the GCIB is analyzed, unlike the dual beam analysis protocol. Then, the 3D OrbiSIMS further enhances the mass resolving power, enabling the direct utilization of GCIB's peptidic fragment generation for protein identification.[8]

However, even if these instruments greatly increase the analysis efficiency, the delivery of sufficient chemically significant ions from a pixel remains a problem even in non-static mode. Therefore, to fully access the benefits of large clusters, there are still challenges that have to be faced and solved:

- Despite the increased lateral resolution resulting from the use of clusters combined to instrument advances, the low ionization probability for the secondary ions, as low as 10^{-5} for most molecules,[3,9] remains limiting.
- The large influence of the chemical environment of a molecule in a sample, known as the matrix effect, can suppress its ionization and therefore hinder its detection.[10−12]
- Topography and preferential sputtering have a large impact on the spectra.

To address these limitations, many efforts have been made in several directions. In addition to the continued search for more efficient projectile sources (*i.e.*, the use of water and acid containing molecular clusters),[2,13] several alternative strategies such as matrix-enhanced SIMS (ME-SIMS)[14−20] and metal-assisted SIMS (MetA-SIMS)[21−24] have been reported to improve sensitivity. For instance, it has been shown that the secondary ion yield increases a lot when tissues are silver- or gold-coated in the case of monoatomic projectile.[23] However, MetA-SIMS has shown some limitation when changing the projectile, in particular a yield decrease using fullerenes (C_{60}^+).[25] In addition, except for the pattern-recognition technique proposed by Sjövall *et al.*[22,24] where the biological samples are imprinted on a silver surface, the metal or matrix deposition process usually affects the integrity of the surface molecules and is not compatible with all biological sample preparations. Reactive vapor exposure can also be applied to the sample.[26,27] Angerer et *al.* showed that trifluoracetic acid exposure combined with a high-energy 40 keV Ar_{4000}^+ beam (using an Ionoptika J105 instrument) can increase a high mass signal and allows the detection of new species in rat brains.[26]

The storing matter (SM) technique, suggested in 2008 by Slodzian and widely tested on polymers[28,29] and metallic samples,[30] split the sputtering and the SIMS ionization process. The SM procedure consists in sputtering the sample onto a collector previously covered by a selected metal layer and analyzing the collector afterward, thereby neutralizing the matrix effect. However, the method was never extended to biological molecules due to the high fragmentation and low sputtering efficiency of the monoatomic Ar^+ beam used. Recently, Lorenz et *al.* showed that large argon clusters could be used to transfer an organic material from one surface onto another with a reduced fragmentation.[31,32] This transfer of intact molecule was extended by our group to larger proteins to develop a soft-landing technique *in situ* a ToF-SIMS instrument. Lysozyme, a protein of 14 kDa, was successfully landed on a silicon wafer with retention of its activity, as was verified afterward via a bioassay in solution.[33] The transfer geometry was also optimized using a 3D printed sample holder (Figure 1).[34]

In this work, the ability of Ar_n^+-GCIB to transfer large intact molecules is used to establish a new method to enhance the SIMS sensitivity and decrease the negative matrix effect. The idea is based on a microvolume expansion of the sample molecules (target) to a collector using large Argon clusters (Figure 1). The dose used for the transfer can be approximatively 100 times higher than the bismuth analysis dose, which is limited due to the subsurface damage created. The second step is to analyze the molecules that are then dispersed on a collector with a chosen matrix or metallic sublayer. The matrix or metallic sublayer are used to increase the signal as in ME-SIMS and MetA-SIMS. Previously, it has been shown that 60% of transferred bradykinin (1060 Da) can be transferred intact using 5 keV Ar_{5000}^+.[34] Therefore, assuming 60% of intact molecules on the collector and complete material collection and considering an enhancement factor of 10 due to the matrix (as reported for some lipids in ref 20), an increase in sensitivity of approximately 600 might be realistic ($= 100 \times 0.6 \times 10$). One has to keep in mind that the transfer of larger molecules and the use of higher cluster energies per atoms (E/n) will decrease this factor. However, the spatial dispersion of the molecules further increases the signal if there is some suppression of ionization within the sample. This signal suppression due to an unfavorable chemical environment was demonstrated for lipids,[10] peptides,[11] and drugs.[35] In these examples, the microvolume expansion approach could be used to improve the understanding of ionization in ToF-SIMS and potentially prevent signal suppression, especially in the cases where only the ionization is affected but not sputtering.

https://doi.org/10.1021/acs.analchem.3c02404
Anal. Chem. 2023, 95, 13620−13628

Here, this new method was first tested on reference lipid samples, namely, phosphatidylcholine (PC) species. They are excellent targets for the evaluation of a new approach because they are highly abundant in tissues (60 mol % of total lipids)[36] and are the main lipids detected in positive mode in ToF-SIMS. Then, mass spectrometry imaging (MSI) studies have shown that ischemic brain tissue can be differentiated from normal brain tissue by the abundance of the PC ion signals.[37−41] However, this change in the PC ion signals is more likely linked to changes in alkali ion concentration in the corresponding tissues than a change in PC concentrations (matrix effect). Moreover, diffusion of PC inside a matrix layer was studied by ToF-SIMS depth profiles when the matrix was transferred[20] or sublimated.[42]

The matrices used here are organic compounds known from matrix-assisted laser desorption/ionization (MALDI). However, the enhancement effect is known to be strongly influenced by the analyte/matrix combination and its concentration ratio.[17] The first part of this work is therefore devoted to the selection of the most promising matrix among a small panel of four acidic matrices known for their high performance on lipids (Figure 1A).[43] Then, the best matrix is sublimated on the collector and two beams (10 keV Ar_{5000}^+ and Ar_{3000}^+) are used to further evaluate the matrix efficiency (Figure 1B). Finally, the method is applied to the analysis of brain tissue and more particularly to the gray matter that contains, among others, PC lipids (Figure 1C).

EXPERIMENTAL SECTION

Lipid Standards and Abbreviations. L-α-Phosphatidylcholine (PC, P3556) was purchased at Sigma-Aldrich (Steinheim, Germany) and dissolved in chloroform (10 mg/mL). The solution contains several PC(x:y) species, which have different fatty acid carbon chain lengths x and different unsaturation degrees y.

The sulfatides identified in the brain are ions designed in the form of ST(FA). FA refers to fatty acid and can be found in tissue with different carbon chain lengths and unsaturations (*e.g.*, ST(24:1) with 24 carbons of which 1 is unsaturated). Fatty acyl moieties can be found with hydroxyl substituents and are denoted with an h (*e.g.*, ST(h24:1)). Sulfatides contain also a dihydroxy long chain base that was d18:1 for the assigned peaks.

Target and Collector Preparation. Targets were thick (0.73 mm) 0.5 × 0.5 cm^2 (Si) wafers. Prior to lipid deposition, the wafers were cleaned for 15 min in a piranha mixture (sulfuric acid/hydrogen peroxide, 2:1), then cleaned with ethanol, and dried with flowing N_2. Targets were prepared by consecutive depositions of 20 μL drops of a stock solution at 10 mg/mL, resulting in a thick dry lipid layer.

Collectors were thin (0.31 mm) 1 × 1 cm^2 (Si) wafers (Neyco S.A., France). Collectors were cleaned just before the deposition of the matrix or just before being inserted in the SIMS, following the same cleaning procedure as for target substrates. The matrix was deposited on the collectors by two means: drop-casting and sublimation. 1,5-Diaminophthalene (DAN), α-cyano-4-hydroxycinnamic acid (CHCA), 2,4,6-trihydroxyacetophenone (THAP), and 9-aminoacridine (9-AA) were purchased as powder from Sigma-Aldrich (Steinheim, Germany) and used without further purification. For CHCA and 9-AA, a stock solution of 0.5 g/L was prepared in water:methanol (1:1). For DAN and THAP, a solution of 0.5 g/L was prepared in water:acetonitrile (1:1). Two microliters these stock solutions was drop-casted on a silicon wafer. CHCA was sublimated owing to a home-built sublimator reaching a vacuum of 4×10^{-5} mbar as described elsewhere.[20] Sublimation of CHCA was performed at 180 °C, and the thickness was controlled by the sublimation time. Surface and thickness of the sublimated layers were characterized by profilometry (Bruker Dektak XT, Bruker UK Ltd.). Unless otherwise specified, all sublimated CHCA layers were sublimated for 1 h at 180 °C from a crucible containing 50 mg of powder. An average thickness of 900 ± 65 nm was then measured with a maximum surface peak height of 15 nm. A gold-coated silicon (Angstrom engineering) and a thin PE foil (additive-free 0.05 mm LDPE, Goodfellow) were also used as alternative collectors. The gold-coated silicon was cleaned with ethanol and hexane and dried with flowing N_2. The PE sheet was cleaned with ethanol and sonicated for 15 min.

Mouse Brain Tissue Sections. After collection, the mouse brains were immersed in a 4% paraformaldehyde (PFA) solution for 6−18 h at room temperature. Afterward, the PFA was replaced with 10% sucrose solution at 4 °C until the sample sank in the vial. The same operation was repeated with a 30% sucrose solution. Then, brains were embedded in carboxymethyl cellulose (CMC) media and conserved at −80 °C. Brain sections (10 μm) were cut in a cryostat microtome and thaw-mounted onto glass slides. Every glass slide was conserved in a −20 °C freezer until utilization.

ToF-SIMS Measurements. A TOF-SIMS V instrument (IONTOF GmbH, Münster, Germany) was used to perform all the experiments. This instrument is equipped with a 30 KeV energy bismuth cluster liquid metal ion gun (LMIG) and an argon gas cluster ion beam (Ar_n^+-GCIB).

The transfer experiment was performed using a polylactic acid (PLA) sample holder. The incident beam angle was set at 45° for maximum sputtering, and the collector was placed on top with a 45° angle to collect a maximum number of molecules. More information on the geometry is available elsewhere.[34] The beam raster area was fixed at 1000 × 1000 μm^2. The alignment was done using the laser that is coaxial with the analyzer. The Ar beam currents were slightly fluctuating from one transfer to another around 6.6 and 7.5 nA for Ar_{3000}^+ and between 1.18 and 1.36 nA for Ar_{5000}^+. The current was measured before the transfer, and each transfer was conducted with a final dose of 2×10^{14} ions to ensure consistent transfer for reproducibility purposes. However, for the first gray matter expansion, a dose of 4.29×10^{14} ions was used to guarantee a sufficient amount of transferred material.

Static analysis of 500 × 500 μm^2 was performed on the topmount sample holder to compare the reference and the collector. Static spectra were acquired with the Bi_5^+ beam (0.07 pA) for 200 s. 2D large mosaic images of the brain and the collector were recorded by moving along the sample surface and recording frames of 500 × 500 μm^2 patches with a pixel size of 128 × 128 by patch.

SIMS depth profiles were recorded with a dual beam method. A 10 keV Ar_{3000}^+ beam was employed to the sputter material with a raster fixed at 700 × 700 μm^2, whereas a 30 keV Bi_5^+ beam, operated with a raster of 200 × 200 μm^2 and centered in the sputtered area, was used to record high mass resolution profiles. The sputter current was adjusted between 0.225 and 0.604 nA depending on the sample thickness, and a charge compensation was conducted using 20 eV electrons for the samples with the matrix.

RESULTS AND DISCUSSION

Evaluation of Matrix Candidates for the Lipid PC. A thick target of drop-casted PC was used to transfer the lipid

https://doi.org/10.1021/acs.analchem.3c02404
Anal. Chem. 2023, 95, 13620−13628

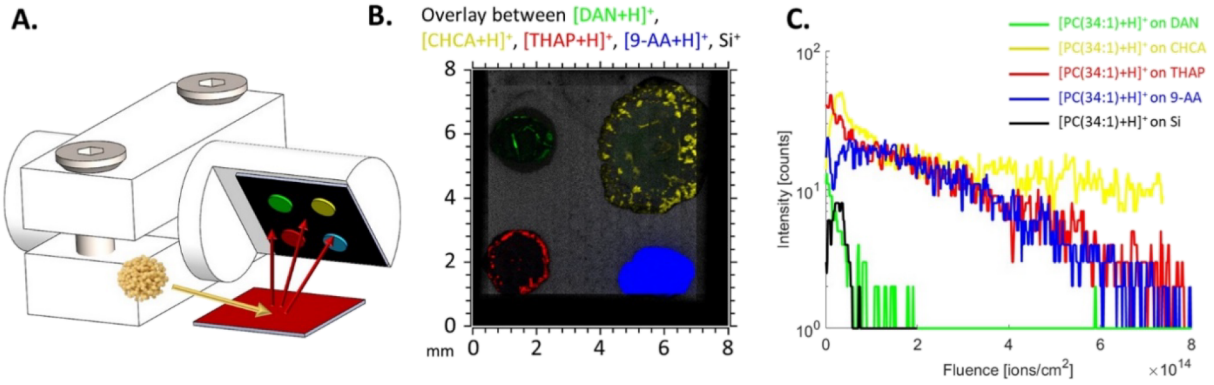

Figure 2. (A) Scheme of the transfer experiment from a target of phosphatidylcholine (red) to a Si collector with four matrices drop-casted: DAN (green), CHCA (yellow), THAP (red), 9-AA (blue). (B) 2D large mosaic image of the collector showing an overlay of the protonated matrix ions. (C) $[PC(34:1) + H]^+$ ion depth profiles performed on a crystal of each matrix and the Si (analysis raster of 50 × 50 μm^2).

sample on a pattern of matrices drop-casted on a collector (Figure 2A). A 10 keV Ar_{5000}^+ beam with a dose of 2×10^{14} ions was used. The goal of the pattern is to quickly select the most appropriate matrix for the compound of interest (PC in our case) with a single transfer under the same conditions. Four matrices were drop-casted on the collector: 1,5-diaminophthalene (DAN), α-cyano-4-hydroxycinnamic acid (CHCA), 2,4,6-trihydroxyacetophenone (THAP), and 9-aminoacridine (9-AA). The choice of these matrices was motivated by their ability to be sublimated and their performance according to the positive polarity of lipids.[43] Figure 2B shows a 2D large image of the collector with an overlay of the protonated ions of the matrices. The size of the spot and the shape of the crystal are highly dependent on the matrix and the solvent used. For instance, the drop of CHCA is more spread on the Si wafer than the others and the THAP crystallizes as a circle at the periphery of the drop. A depth profile was obtained on a crystal of each matrix, and the $[PC(34:1) + H]^+$ signal, the most intense peak of PC, is plotted as a function of the sputtering dose in Figure 2C. Compared to the signal on Si (black line), all the matrices improve the signal. Moreover, the PC seemed to diffuse inside the crystals except for DAN, assuming a similar sputtering rate for all the matrices. For the following experiments, CHCA will be used for two reasons, its sublimation creates homogeneous layers with minimal surface roughness (see Figures S1 and S7A) and the matrix offers the largest signal enhancement at the surface and deeper into the crystal.

Transfer of PC on Si and Sublimated CHCA. To confirm and quantify the signal enhancement due to the transfer on a matrix, a collector half-coated by sublimated CHCA, the best performing matrix, was prepared. This collector allows us to compare the expansion on Si and CHCA with the same transfer conditions. Then, 10 keV Ar_{5000}^+ and 10 keV Ar_{3000}^+ were used to transfer the PC reference and the experiment was reproduced three times for each beam. The same dose of 2×10^{14} ions was used to compare the impact of the energy per atom (E/n) of the transfer Ar clusters on the final secondary ion yield of PC. The mass distributions of these respective beams are shown in the SI, Figure S2. Figure 3B shows the main PC ion species $[PC(x:y) + H]^+$ image of the collector after a transfer with Ar_{3000}^+. The spectra are mainly dominated by protonated PC species rather than being cationized by potassium or sodium, as is the case in brain tissues, owing to the lower alkali ion concentration in the standard samples. The signal is much more pronounced on the right side where the silicon was covered with sublimated CHCA.

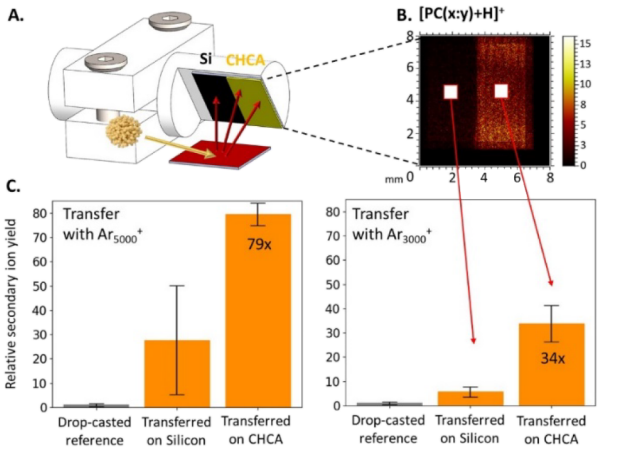

Figure 3. (A) Scheme of the transfer experiment from a target of phosphatidylcholine (red) to a Si collector half-coated with CHCA (yellow). (B) $[PC(x:y) + H]^+$ ion large image of the collector. The white squares indicate areas where 500 × 500 μm^2 static analyses were performed. (C) Relative secondary ion yield for the ions $[PC(x:y) + H]^+$ on the silicon side and the CHCA side for two transfers (Ar_{5000}^+ and Ar_{3000}^+).

However, the matrix only increases the signal of the molecular ions in positive mode. Looking at the fragments, the PC head group fragment (PC HG, m/z 184) is less intense on the CHCA side in positive mode and the fatty acid (FA) ion signals (such as $[FA(16:0)-H]^-$) are strongly reduced in negative mode. The 2D large images of these ions can be found in the SI, Figure S3.

After the large-area image, 500 × 500 μm^2 static analyses were performed on the target, on the drop-casted reference, and on the silicon side and the CHCA side of the collector. The respective mass spectra upon one transfer with Ar_{5000}^+ can be found in the SI, Figure S4 (The assigned peaks are summed in $[PC(x:y) + H]^+$). The results of all the transfers are summarized as histograms in Figure 3C, showing the secondary ion yield computed and normalized to that of the drop-casted reference. The results and the error bars correspond, respectively, to an average of three transfers for each beam and to the standard deviation resulting from it. There is a slight increase when the PC is transferred on Si and the increasing factor rises to 79-fold when the lipid is transferred with Ar_{5000}^+ to 34-fold when transferred with Ar_{3000}^+. The more intense signal obtained with Ar_{5000}^+ can be explained by the fact that the fragmentation induced during the sputtering is a function of the energy per

https://doi.org/10.1021/acs.analchem.3c02404
Anal. Chem. 2023, 95, 13620−13628

atom ratio (E/n) in the cluster projectiles.[44−46] Therefore, a higher abundance of intact PC ions compared to the fragments can be expected on the collector.

The method offers an additional advantage in situations where the analysis beam used is constrained by the static limit, as is the case with the standard analytical beams Au_3^+, Bi_3^+, and Bi_5^+ on most SIMS instrument. Indeed, as a consequence of the expansion, the analysis can be performed on a 196 times larger area, which increases the final primary ion dose that can be used without causing any damage (in this experiment, the transfer raster area is 0.25 mm^2 against 49 mm^2 for the entire collector). However, it should be noted that achieving such coverage requires an extended analysis time. Combined to the improved sensitivity resulting from the underlying matrix, the potential signal increase reaches four orders of magnitude for Ar_{5000}^+ (= 196 × 79) and three orders for Ar_{3000}^+ transfers (= 196 × 34). These values possess a partial theoretical nature since only one of the two multiplicated factors is actually measured. To validate the applicability of the area expansion factor as a reliable approximation of the increase, a large coverage experiment was conducted, as depicted in the SI, Figure S5. This first experiment is a proof of concept of the method and an optimization of the matrix thickness[19] along with judicious selection of the most efficient matrix for the studied system[14] could further increase the enhancement factor.

Effects of the Substrate and the Matrix Layer Thickness. To gain a deeper understanding of the signal enhancement, two depth profiles were performed on a collector depicted in Figure 3 upon transfer with Ar_{3000}^+ (one on the CHCA side and another one on the Si side). In Figure 4A, the depth profile is divided into four areas: the first interface (blue), within the matrix bulk (yellow), at the interface between the organic layer and the silicon (blue), and in the silicon bulk (black). In the matrix layer, there is a large diffusion of PC lipids and an increase in signal due to the beneficial proton donor environment provided by the CHCA matrix. At the interface between the organic layer and the silicon (interface #2), there is a systematic bump of the ion signals. This increase in signal intensity at the interface can be described as the difference between the maximum of intensity and the intensity in the bulk. Since the molecular ion $[PC(34:1) + H]^+$ has a higher increase of 3.6 compared to the 2.0 for the fragment PC HG (m/z 184), this phenomenon cannot be only attributed to a fragmentation effect. Indeed, it has been shown by Cristaudo et *al.*[47] that the ion yield enhancement at the interface between an organic layer and a hard substrate (*e.g.*, silicon) is caused by the concomitance of three factors: (i) ionization and matrix effect change, (ii) sputtering, and (iii) fragmentation increase at the interface. The last two factors are linked to energy confinement between soft and hard substrates. The microvolume expansion approach can take advantage of this increase in the ion signal at the interface if a thin layer of biomolecules is transferred onto a hard substrate (as is the case of the transfer onto Si in Figure 4B). However, the use of a matrix seems to be even more beneficial.

Looking at the fragmentation, the signal of the PC HG ion is more intense after the transfer on both sides of the collector (SI, Figure S6A). This can be related to the increase in the ion signal of the fragment but also to the fragmentation induced during the transfer with the Ar cluster beam. However, the $[PC(34:1) + H]^+$/PC HG secondary ion yield ratio is greatly increased upon transfer on CHCA (SI, Figure S6B), showing that, in agreement with other studies,[16,48,49] the matrix enhances the formation of

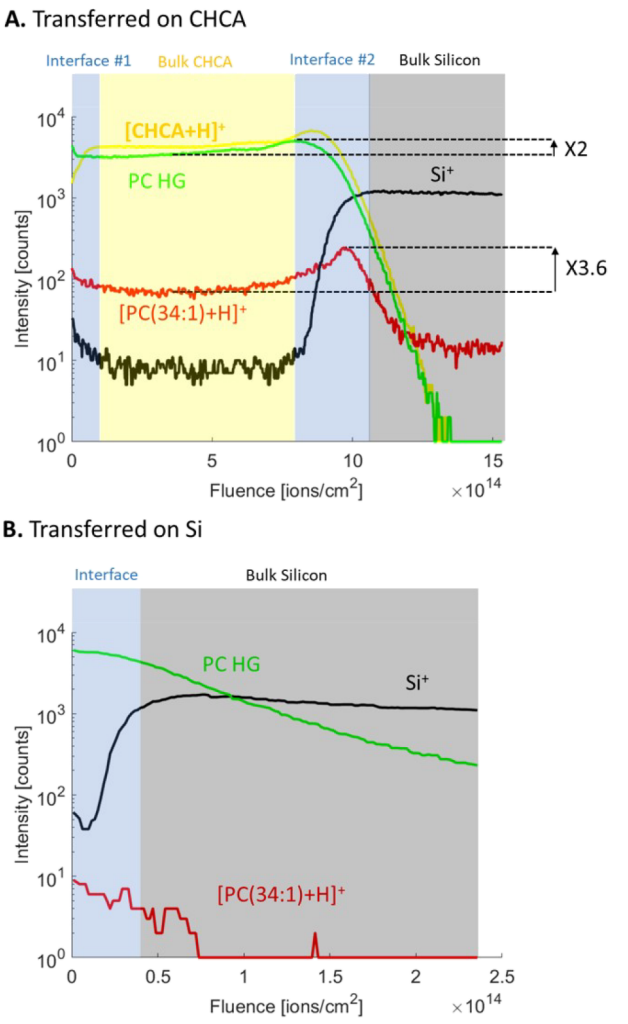

Figure 4. Positive depth profiles of PC transferred on (A) CHCA and (B) Si. The CHCA bulk region is in yellow, the interfaces in blue, and the bulk silicon in black. The increasing factor between the bulk and the interface maximum are shown for (A). PC HG is the head group fragment at m/z 184.

$[M + H]^+$ ions through at least two mechanisms, by reducing the fragmentation and donating protons.

The enhancement in secondary ion formation is strongly dependent upon the matrix employed but also upon the matrix/analyte concentration ratio. In the profile of Figure 4A, the lipids diffuse in the whole matrix layer. Hence, it is crucial to determine the ideal thickness that would result in an optimal matrix/analyte concentration ratio. To obtain this value, two parameters can be tuned: (i) the amount of analyte transferred, which is linearly proportional to the transfer dose, and (ii) the matrix thickness controlled during the sublimation. To achieve the best results, it is essential to optimize these parameters, particularly when the analyte's detection is challenging. To illustrate the importance of controlling the matrix/analyte ratio, the Ar_{3000}^+ transfer of the PC experiment of Figure 3B was reproduced with the same dose but on a five times thinner matrix layer of 177.9 ± 9.5 nm. The relative secondary ion yields at the surface and depth profiles are compared in the SI, Figure S7. Once again, the $[PC(x:y) + H]^+$ signal is increased (11 times) but the matrix layer seems to be saturated in lipid molecules because a top layer of transferred material is now deposited at the surface. Therefore, the matrix/analyte ratio is not the same at the

https://doi.org/10.1021/acs.analchem.3c02404
Anal. Chem. 2023, 95, 13620−13628

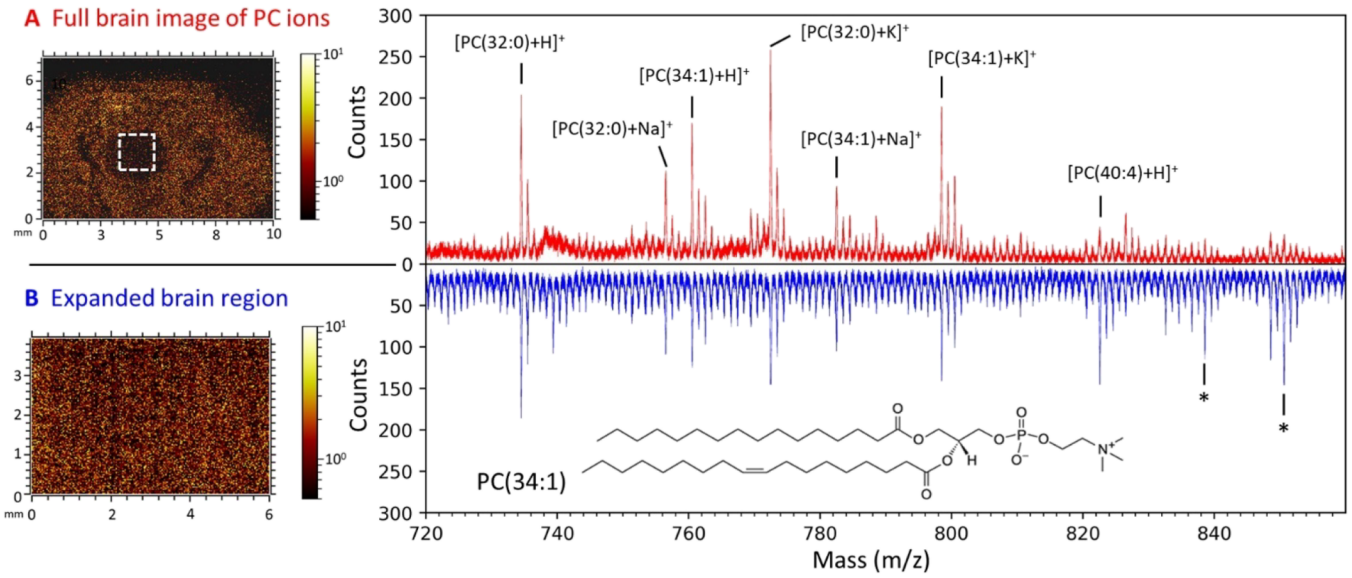

Figure 5. Images from cumulative PC ion signals $[M + H]^+$, $[M + Na]^+$, and $[M + K]^+$ for (A) the mouse brain slice cut used as the target and (B) the collector after transfer. The mass spectra on the right correspond to the brain total image (red) and the collector subregion image (blue). An asterisk (*) is used to highlight the intense unassigned peaks. The chemical formula of PC(34:1) is illustrated. A dotted white line outlines the sputtered area.

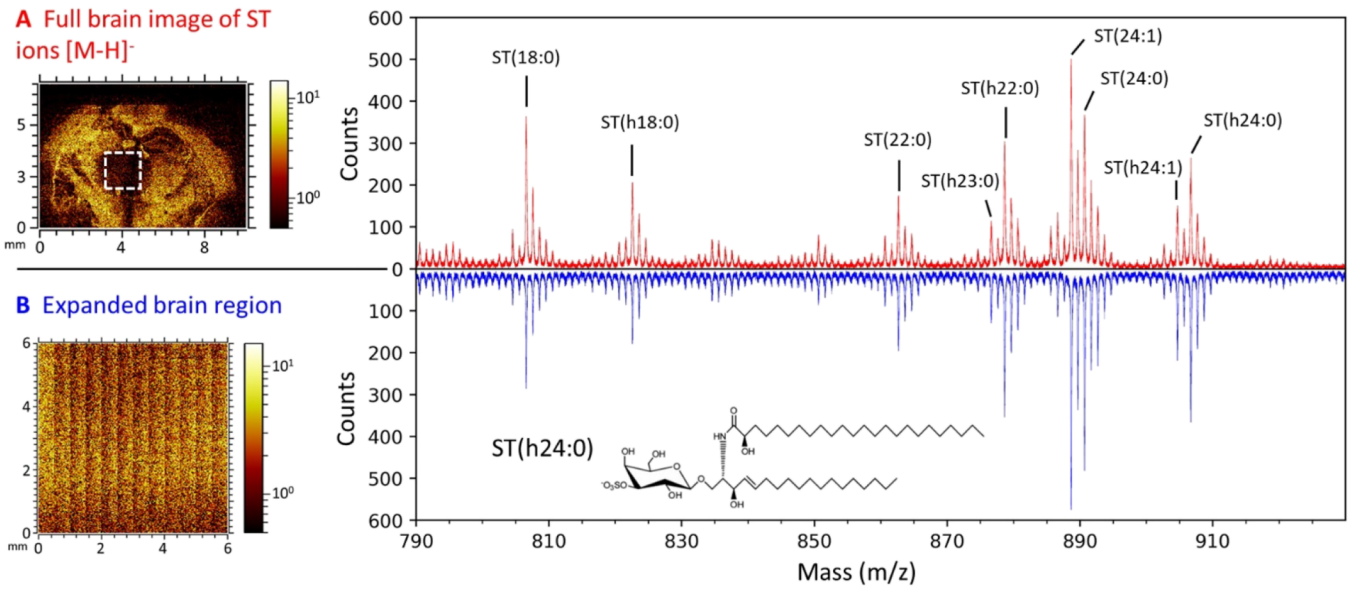

Figure 6. Images from cumulative sulfatides species $[M\text{-}H]^-$ for (A) the mouse brain slice cut used as the target and (B) the collector after transfer. The spectra on the right correspond to the brain total image (red) and the collector total image (blue). The chemical formula of ST(h24:0) is illustrated. A dotted white line outlines the sputtered area.

surface compared to the matrix bulk, decreasing the molecular signal intensity.

Expansion of a Mouse Brain Tissue Microvolume. Finally, a brain tissue was transferred with 10 keV Ar_{5000}^+ (dose = 4.29×10^{14} ions) on a Si collector. This first microvolume expansion of tissue was performed with a larger dose than the one used for the reference samples owing to the anticipated significantly lower PC lipid concentration in the brain as opposed to the pure PC target. Moreover, molecular entanglement is expected to reduce the sputtering rate for the brain tissue.[21] Figure 5A illustrates the total brain image of the protonated or cationized PC ions, with either potassium or sodium, and the corresponding positive secondary ion mass spectrum in red. The peaks in the brain reference were assigned using previous ToF-SIMS[36,50] and MALDI[51] studies. The raster of 1 mm^2, which delineates the transferred region, is discernible within the cerebral cortex (gray matter) center. Figure 5B displays a subregion image (6 × 4 mm) of the Si collector subsequent to the transfer process, along with the corresponding positive mass spectrum in blue. Upon comparison of the mass spectra, a notable observation is that the spectra exhibit a high degree of similarity across all identified PCs. Nevertheless, unassigned peaks at m/z 838.6, 850.6, and 866.6, which were not observed on the Si reference, were found to be more intense after the transfer. Assignment suggestions from LIPID MASS can be found in the SI, Table S1. In addition, the resemblance is also observed in other mass regions of the spectra, including the

https://doi.org/10.1021/acs.analchem.3c02404
Anal. Chem. 2023, 95, 13620−13628

Table 1. Lipid Ratios of PC (Positive Mode) and ST (Negative Mode) after Transfer of a Microvolume of Mouse Brain Gray Matter on Si and CHCA[a]

Gray matter lipids				Ratios on Si		Ratios on CHCA	
label	Formula	Mass (m/z)	Species	0.25 mm^2	Scaled to 64 mm^2	0.25 mm^2	Scaled to 64 mm^2
Positive mode							
PC HG	$C_5H_{15}PNO_4^+$	184.08	$[M+H]^+$	0.44±0.18	112±46	0.52±0.08	133±20
PC(32:0)	$C_{40}H_{81}NO_8P^+$	734.56	$[M+H]^+$	2.02±0.07	517±18	2.07±0.24	530±61
PC(32:0)	$C_{40}H_{80}NO_8PNa^+$	756.54	$[M+Na]^+$	1.21±0.22	309±56	1.47±0.04	376±10
PC(34:1)	$C_{42}H_{83}NO_8P^+$	760.53	$[M+H]^+$	2.34±0.12	599±31	2.48±0.24	635±61
PC(32:0)	$C_{40}H_{80}NO_8PK^+$	772.51	$[M+K]^+$	0.70±0.14	179±36	0.82±0.10	210±26
PC(34:1)	$C_{42}H_{82}NO_8PNa^+$	782.51	$[M+Na]^+$	3.45±0.26	883±67	3.68±0.50	942±128
PC(34:1)	$C_{42}H_{82}NO_8K^+$	798.48	$[M+K]^+$	2.00±0.03	512±8	2.21±0.31	566±79
PC(40:4)	$C_{48}H_{88}NO_7PH^+$	822.52	$[M+H]^+$	9.60±1.54	2458±294	9.99±0.46	2557±118
*	—	838.62	—	10.85±0.95	2778±243	10.17±0.35	2604±90
*	—	850.66	—	12.2±2.52	3123±645	11.15±0.38	2854±97
*	—	866.64	—	12.80±0.85	3277±218	12.62±1.34	3230±343
Negative mode							
FA(16:0)	$C_{16}H_{31}O_2^-$	255.19	$[M-H]^-$	0.32±0.02	82±5	0.08±0.03	20±8
FA(18:1)	$C_{18}H_{33}O_2^-$	281.21	$[M-H]^-$	0.37±0.01	95±3	0.15±0.02	38±5
FA(18:0)	$C_{18}H_{35}O_2^-$	283.22	$[M-H]^-$	0.359±0.05	92±13	0.20±0.05	51±13
ST(18:0)	$C_{42}H_{80}NO_{11}S^-$	806.47	$[M-H]^-$	1.21±0.02	310±5	0.64±0.10	164±26
ST(h18:0)	$C_{42}H_{80}NO_{12}S^-$	822.48	$[M-H]^-$	0.96±0.02	246±5	0.55±0.06	141±15
ST(22:0)	$C_{46}H_{88}NO_{11}S^-$	862.59	$[M-H]^-$	1.93±0.06	494±15	1.04±0.28	266±72
ST(h22:0)	$C_{46}H_{88}NO_{12}S^-$	878.52	$[M-H]^-$	1.24±0.01	317±3	0.60±0.17	154±44
ST(24:1)	$C_{48}H_{90}NO_{11}S^-$	888.57	$[M-H]^-$	1.52±0.10	389±26	0.94±0.03	241±8
ST(24:0)	$C_{48}H_{92}NO_{11}S^-$	890.54	$[M-H]^-$	1.56±0.05	399±26	0.78±0.22	200±56
ST(h24:0)	$C_{48}H_{92}NO_{12}S^-$	906.54	$[M-H]^-$	1.21±0.07	310±18	0.63±0.18	161±46

[a]Peaks are sorted by increasing mass (m/z). The ratios are normalized to the gray matter reference and color coded (below 1 in red and above 1 in green). An asterisk (*) for the label indicates intense ions that where not detected on cleaned reference Si and reference CHCA.

region of amino acid fragments, fatty acids, and cholesterol (see the SI, Figures S8−S10).

In negative ion mode, the detection of lipids such as sulfatides (STs) with varying fatty acid chain lengths was achieved. Figure 6 shows the total images of the ST negative ions $[M-H]^-$ and their respective mass spectra obtained from the brain reference (red) and the Si collector (blue). Once more, the mass spectra exhibit a very close similarity for all the STs, and no new peaks are observed in this mass range compared to the positive ion mode.

The microvolume expansion of the gray matter was successful, as evidenced by the matching spectra of the collector and the brain with minimal added complexity. This indicates that the Ar_n^+-GCIB beam is able to expand the molecules without causing significant damage and that the entanglement of the molecules in the brain tissue is not a hindrance for the microvolume expansion approach. Therefore, with the aim of increasing the signal of PC protonated ionic species, a second transfer of gray matter was performed on a collector half-coated with sublimated CHCA under the same conditions as for the previous reference transfers (10 keV Ar_{5000}^+ with a dose of 2×10^{14} ions). Table 1 provides a summary of the PC and ST ionic species detected in positive and negative mode, respectively. The secondary ion yields are computed and normalized to that of the gray matter reference and are provided as two ratios. The initial ratio was obtained from an average of three separate 500×500 μm^2 analysis performed on the samples. Then, the second ratio was computed by scaling the initial ratio to the total collector area (*i.e.*, multiplied by a factor 256). This factor comes from the fact that the analysis can be performed on the entire 64 mm^2 collector area, without being restricted to a 500×500 μm^2 raster.

For PC ions in positive mode, the signal is increased for almost all species, but the CHCA matrix does not lead to any improvement over bare silicon. Several factors have to be considered to explain this result. First, a suboptimal ratio of analyte to matrix, as explained earlier, and then, compared to the case of the pure PC standard, a substantial amount of sodium and potassium ions are also transferred and consequently present on the collector surface, leading to the creation of adduct ions ($[M + Na]^+$ and $[M + K]^+$). The enhancement of these adduct ions is comparable to one of the protonated ions in the transferred brain tissue. However, when scaled to the collector size, the observed increase becomes more significant as illustrated in the last column of Table 1.

In negative mode, the formation of $[M-H]^-$ ions for ST lipids decreases when embedded in the matrix. This result was anticipated since CHCA is a cinnamic acid of pK_a of 1.17 and proton donation plays a major role in the formation of molecular ions for those kinds of matrices. Previous studies have demonstrated a correlation between decreasing pK_a and increasing protonated positive ion, especially for halogen-substituted cinnamic acid derivatives.[49]

The microvolume expansion technique may benefit from the increase in the ion signal at the interface between the organic layer and a hard substrate, which could explain the observed increase in signal despite the reduction in available molecules per unit area after expansion. To verify this hypothesis, mouse brain gray matter was also transferred onto another hard surface (Au-coated silicon) and compared to a soft surface (PE foil). A table summarizing the ionization ratios of PC and ST ionic species after transfer can be found in the SI, Table S2. Depth profiles performed on both surfaces are given in the SI, Figure S11. The first striking feature is that the signal is reduced by about an order of magnitude on the PE surface compared to the Au surface. Indeed, on PE, there is an increase only for the unassigned peaks that were not detected on the references. These ions can be molecules that were suppressed in the brain before expansion. Compared to silicon, the increase on Au is similar for the PC ions but lower for the ST ions in negative mode. However, no Au-cationized PCs were identified, implying that Au-coated silicon does not offer any additional benefits over silicon for the targeted lipids.

Spatial Resolution of the Method. In the context of analyzing biological materials, a limitation of the microvolume expansion technique is that it appears to compromise the ToF-

https://doi.org/10.1021/acs.analchem.3c02404
Anal. Chem. 2023, 95, 13620−13628

SIMS instrument's ability to achieve high lateral and depth resolution due to the initial step of GCIB sputtering. However, it was already challenging to achieve sub-100 nm lateral resolution using directly Bi primary ion clusters[52] due to the low ionization probability of many biologically relevant molecules. Moreover, a lot of work has been devoted to optimizing the capabilities of the GCIB. For instance, intact phospholipids were detected with a high energy (~40 keV) $Ar_{1000-4000}^+$ cluster beams focused on 3 μm.[53] Alternative gases such as $(CO_2)_n$-GCIB or chemical doping also allowed a better focus down to 1 μm^2. Therefore, the lateral resolution of the microvolume method is not as good as the direct analysis by Bi primary ion clusters, but it is still possible to reach the micrometer, as long as the beam remains capable of desorbing intact molecules. Nonetheless, the final useful lateral resolution of the method will be dependent not only on the GCIB beam's focusing ability but also on the desired depth resolution. To illustrate this point, one can assume that a volume of 1 μm^3 is needed to expand enough molecules on the collector. If the desired lateral resolution is 2 μm, then the useful depth resolution will also be 0.25 μm to reach the required expanded volume of 1 μm^3. There is a trade-off between lateral and depth resolution that will depend on the number of intact molecules needed on the collector.

CONCLUSIONS AND FUTURE PROSPECTS

We have developed a new method to increase the sensitivity in SIMS using the molecular transfer by argon clusters. The ability of large Ar clusters to transfer unfragmented molecules from a target to a collector was used for the first time on phosphatidylcholine (PC) and gray matter of the mouse brain. Using a PLA 3D printed sample holder and an acidic matrix array, CHCA was quickly selected as the most promising matrix among four other MALDI matrices. Upon expansion of pure PC on a sublimated layer of CHCA, the signal exhibits an increase of at least three orders of magnitude when scaled to the area of the collector. The matrix plays an important role by reducing the fragmentation and acting as a proton donor, but signal enhancements are also measured on bare silicon. This beneficial effect in the case of silicon comes from the ion yield enhancement at the interface between a thin organic layer and a hard surface (the signal is an order of magnitude higher after expansion onto silicon and Au-coated silicon compared to a soft PE sheet). Then, when the microvolume expansion is applied to the gray matter of the brain, the chemical information in the considered mass is fully preserved throughout the transfer and analysis. The PC ion species signals of the gray matter were enhanced by expansion on a layer of CHCA. Further optimization of the matrix/analyte ratio can increase even more the signal.

The microvolume expansion is compatible with any tissue sample preparation since the matrix is not directly applied on the sample. This can be particularly beneficial in analyzing white matter, where artifacts are caused by the high concentration of cholesterol.[27,42] Changes in the sample preparation such as tape-supporting or frozen-hydrated samples[54] reduce these artifacts and can be combined with our method. In addition, spatial separation of the cholesterol from the other lipids on the collector may be beneficial in reducing the negative matrix effect. The main limitation is the trade-off that has to be evaluated between the focusing capacity of the GCIB and the desired depth resolution.

Future prospects include utilizing this method to identify molecules, such as drugs, in tissues where low detection efficiency or the matrix effect may hinder ToF-SIMS analysis. Additionally, model tissues, such as the lyophilized bovine liver tissue standard,[35] can also be employed to determine the limit of detection of a doped drug and to choose the most appropriate matrix. To expedite the screening process of various matrix candidates, it is recommended to transfer them onto a patterned surface. This method can quickly identify the optimal matrix from a larger pool. Additionally, a comprehensive matrix optimization can be conducted by evaluating the sputtering yield, the ionization yield, and the damage cross section for a wider range of matrices. With this aim in mind, potential new matrix candidates, including halogen-substituted cinnamic acid derivatives[49] or acid molecules without aromatic cycles, should be explored.

Interestingly, large argon clusters are able to desorb and transfer larger intact molecules than those that can be ionized and detected by ToF-SIMS, such as lysozyme.[33,46] Therefore, the ability of MALDI to ionize larger molecules than SIMS could be very beneficial to uncover a larger spectrum of transferred biomolecules than those visible in SIMS. The other advantage is that, per the size of the interaction volume, MALDI can ablate the entire thickness of the matrix layer and therefore readily take advantage of all the molecular signals available on the collector and not just the surface like static SIMS analyses (see the diffusion profiles of Figure 4). The fusion of ToF-SIMS' high resolution with the increased mass range provided by MALDI should result in a powerful combination.

ASSOCIATED CONTENT

Supporting Information

The Supporting Information is available free of charge at https://pubs.acs.org/doi/10.1021/acs.analchem.3c02404.

Figure S1: Comparison between drop-casted and sublimated CHCA; Figure S2: Cluster mass distributions; Figure S3: Collector 2D large mosaic images; Figure S4: Spectra comparison of drop-casted reference of PC and expanded PC upon Ar_{5000}^+ transfer; Figure S5: PC comparison between target and collector images; Figure S6: Ratio fragment and molecular PC ion; Figure S7: profiles through CHCA of different thicknesses; Figure S8: Reference and collector amino acid mass spectra; Figure S9: Reference and collector fatty acid mass spectra; Figure S10: Reference and collector cholesterol mass spectra; Table S1: Assignment suggestions for the unassigned peaks; Table S2: Lipid ratios of PC and ST on PE and Au; Figure S11: Profiles on Au and PE after PC transfer (PDF)

AUTHOR INFORMATION

Corresponding Author

Arnaud Delcorte − *Institute of Condensed Matter and Nanosciences, Université catholique de Louvain, 1348 Louvain-la-Neuve, Belgium;* orcid.org/0000-0003-4127-8650; Email: arnaud.delcorte@uclouvain.be

Authors

Benjamin Tomasetti − *Institute of Condensed Matter and Nanosciences, Université catholique de Louvain, 1348 Louvain-la-Neuve, Belgium;* orcid.org/0009-0008-7986-6144

Clément Lauzin − *Institute of Condensed Matter and Nanosciences, Université catholique de Louvain, 1348*

Louvain-la-Neuve, Belgium; orcid.org/0000-0001-5044-5137

Complete contact information is available at: https://pubs.acs.org/10.1021/acs.analchem.3c02404

Notes

The authors declare no competing financial interest.

■ ACKNOWLEDGMENTS

The authors acknowledge the financial support by the Fédération Wallonie Bruxelles, through the project "iBEAM" funded by its research program "Actions de Recherche Concertées" (Convention No. 18/23-090) and by the Belgian National Foundation for Scientific Research (FNRS). Véronique Préat laboratory is thanked for providing the brain tissue samples. B.T. is a research fellow (ASP) of the FNRS. A.D. is a Research Director of the FNRS.

■ REFERENCES

(1) Fletcher, J. S.; Vickerman, J. C. *Anal. Bioanal. Chem.* **2010**, *396*, 85−104.
(2) Tian, H.; Sheraz Née Rabbani, S.; Vickerman, J. C.; Winograd, N. *Anal. Chem.* **2021**, *93*, 7808−7814.
(3) Vickerman, J. C. 1 ToF-SIMS — An Overview. In *"ToF-SIMS—an overview." ToF-SIMS: surface analysis by mass spectrometry*; 2001; pp. 1−40, DOI: 10.50968/vivaorigino.36.2_20.
(4) Jones, E. A.; Lockyer, N. P.; Vickerman, J. C. *Anal. Chem.* **2008**, *80*, 2125−2132.
(5) Bich, C.; Havelund, R.; Moellers, R.; Touboul, D.; Kollmer, F.; Niehuis, E.; Gilmore, I. S.; Brunelle, A. *Anal. Chem.* **2013**, *85*, 7745−7752.
(6) Shon, H. K.; Yoon, S.; Moon, J. H.; Lee, T. G. *Biointerphases* **2016**, *11*, No. 02A321.
(7) Passarelli, M. K.; Pirkl, A.; Moellers, R.; Grinfeld, D.; Kollmer, F.; Havelund, R.; Newman, C. F.; Marshall, P. S.; Arlinghaus, H.; Alexander, M. R.; West, A.; Horning, S.; Niehuis, E.; Makarov, A.; Dollery, C. T.; Gilmore, I. S. *Nat. Methods* **2017**, *14*, 1175−1183.
(8) Kotowska, A. M.; Trindade, G. F.; Mendes, P. M.; Williams, P. M.; Aylott, J. W.; Shard, A. G.; Alexander, M. R.; Scurr, D. J. *Nat. Commun.* **2020**, *11*, 1−8.
(9) Popczun, N. J.; Breuer, L.; Wucher, A.; Winograd, N. *J. Am. Soc. Mass Spectrom.* **2017**, *28*, 1182−1191.
(10) Sostarecz, A. G.; Cannon, D. M.; McQuaw, C. M.; Sun, S.; Ewing, A. G.; Winograd, N. *Langmuir* **2004**, *20*, 4926−4932.
(11) Jones, E. A.; Lockyer, N. P.; Kordys, J.; Vickerman, J. C. *J. Am. Soc. Mass Spectrom.* **2007**, *18*, 1559−1567.
(12) Alnajeebi, A. M.; Vickerman, J. C.; Lockyer, N. P. *Biointerphases* **2016**, *11*, No. 02A317.
(13) Sheraz née Rabbani, S.; Barber, A.; Fletcher, J. S.; Lockyer, N. P.; Vickerman, J. C. *Anal. Chem.* **2013**, *85*, 5654−5658.
(14) Svara, F. N.; Kiss, A.; Jaskolla, T. W.; Karas, M.; Heeren, R. M. A. *Anal. Chem.* **2011**, *83*, 8308−8313.
(15) Delcorte, A. *Appl. Surf. Sci.* **2006**, *252*, 6582−6587.
(16) Luxembourg, S. L.; McDonnell, L. A.; Duursma, M. C.; Guo, X.; Heeren, R. M. A. *Anal. Chem.* **2003**, *75*, 2333−2341.
(17) Adriaensen, L.; Vangaever, F.; Lenaerts, J.; Gijbels, R. *Rapid Commun. Mass Spectrom.* **2005**, *19*, 1017−1024.
(18) Dowlatshahi Pour, M.; Malmberg, P.; Ewing, A. *Anal. Bioanal. Chem.* **2016**, *408*, 3071−3081.
(19) Körsgen, M.; Pelster, A.; Vens-Cappell, S.; Roling, O.; Arlinghaus, H. F. *Surf. Interface Anal.* **2016**, *48*, 34−39.
(20) Moshkunov, K.; Tomasetti, B.; Daphnis, T.; Delmez, V.; Vanvarenberg, K.; Préat, V.; Lorenz, M.; Quanico, J.; Baggerman, G.; Lemiere, F.; Dupont, C.; Delcorte, A. *Analyst* **2021**, *146*, 6506−6519.
(21) Delcorte, A.; Médard, N.; Bertrand, P. *Anal. Chem.* **2002**, *74*, 4955−4968.
(22) Sjövall, P.; Lausmaa, J.; Nygren, H.; Carlsson, L.; Malmberg, P. *Anal. Chem.* **2003**, *75*, 3429−3434.
(23) Nygren, H.; Johansson, B. R.; Malmberg, P. *Microsc. Res. Tech.* **2004**, *65*, 282−286.
(24) Malmberg, P.; Nygren, H.; Sjövall, P.; Lausmaa, J. *Spectroscopy* **2004**, *18*, 503−511.
(25) Delcorte, A.; Yunus, S.; Wehbe, N.; Nieuwjaer, N.; Poleunis, C.; Felten, A.; Houssiau, L.; Pireaux, J. J.; Bertrand, P. *Anal. Chem.* **2007**, *79*, 3673−3689.
(26) Angerer, T. B.; Dowlatshahi Pour, M.; Malmberg, P.; Fletcher, J. S. *Anal. Chem.* **2015**, *87*, 4305−4313.
(27) Angerer, T. B.; Mohammadi, A. S.; Fletcher, J. S. *Biointerphases* **2016**, *11*, No. 02A319.
(28) Philipp, P.; Douhard, B.; Lacour, F.; Wirtz, T.; Houssiau, L.; Pireaux, J. J.; Migeon, H. N. *Appl. Surf. Sci.* **2008**, *255*, 866−869.
(29) Becker, N.; Wirtz, T.; Migeon, H. N. *Surf. Interface Anal.* **2011**, *43*, 413−416.
(30) Miśnik, M.; Konarski, P.; Zawada, A.; Ażgin, J. *Nucl. Instrum. Methods Phys. Res. B* **2019**, *450*, 153−156.
(31) Lorenz, M.; Shard, A. G.; Counsell, J. D. P.; Hutton, S.; Gilmore, I. S. *J. Phys. Chem. C* **2016**, *120*, 25317−25327.
(32) Lorenz, M.; Zhang, J.; Shard, A. G.; Vorng, J.-L.; Rakowska, P. D.; Gilmore, I. S. *Anal. Chem.* **2021**, *93*, 3436−3444.
(33) Delmez, V.; Degand, H.; Poleunis, C.; Moshkunov, K.; Chundak, M.; Dupont-Gillain, C.; Delcorte, A. *J. Phys. Chem. Lett.* **2021**, *12*, 952−957.
(34) Delmez, V.; Tomasetti, B.; Daphnis, T.; Poleunis, C.; Lauzin, C.; Dupont-Gillain, C.; Delcorte, A. *ACS Appl. Bio Mater.* **2022**, *5*, 3180−3192.
(35) Vorng, J.-L.; Kotowska, A. M.; Passarelli, M. K.; West, A.; Marshall, P. S.; Havelund, R.; Seah, M. P.; Dollery, C. T.; Rakowska, P. D.; Gilmore, I. S. *Anal. Chem.* **2016**, *22*, 11028−11036.
(36) McArthur, S. L. *Surf. Interface Anal.* **2006**, *38*, 1380−1385.
(37) Koizumi, S.; Yamamoto, S.; Hayasaka, T.; Konishi, Y.; Sugiura, Y.; Setou, M.; Namba, H. *Neuroscience* **2010**, *168*, 219−225.
(38) Hankin, J. A.; Farias, S. E.; Barkley, R. M.; Heidenreich, K.; Frey, L. C.; Hamazaki, K.; Kim, H.-Y.; Murphy, R. C *J. Am. Soc. Mass Spectrom.* **2011**, *22*, 1014.
(39) Norris, J. L.; Caprioli, R. M. *Chem. Rev.* **2013**, *4*, 2309−2342.
(40) Wang, H. J.; Wu, H.; Tsai, P.; Liu, C. B. *Anal. Bioanal. Chem.* **2012**, *404*, 113−124.
(41) Lanekoff, I.; Stevens, S. L.; Stenzel-Poore, M. P.; Laskin, J. *Analyst* **2014**, *139*, 3528−3532.
(42) Van Nuffel, S.; Elie, N.; Yang, E.; Nouet, J.; Touboul, D.; Chaurand, P.; Brunelle, A. *Anal. Chem.* **2018**, *90*, 1907−1914.
(43) Thomas, A.; Charbonneau, J. L.; Fournaise, E.; Chaurand, P. *Anal. Chem.* **2012**, *84*, 2048−2054.
(44) Rabbani, S.; Barber, A. M.; Fletcher, J. S.; Lockyer, N. P.; Vickerman, J. C. *Anal. Chem.* **2011**, *83*, 3793−3800.
(45) Delcorte, A.; Cristaudo, V.; Lebec, V.; Czerwinski, B. *Int. J. Mass Spectrom.* **2014**, *370*, 29−38.
(46) Bertolini, S.; Delcorte, A. *Appl. Surf. Sci.* **2023**, *631*, No. 157487.
(47) Cristaudo, V.; Poleunis, C.; Laha, P.; Eloy, P.; Hauffman, T.; Terryn, H.; Delcorte, A. *Appl. Surf. Sci.* **2021**, *2021*, No. 147716.
(48) Wu, K. J.; Odom, R. W. *Anal. Chem.* **1996**, *68*, 873−882.
(49) Pohkrel, Y.; Adolphs, T.; Peterson, R. E.; Allebrod, U.; Ravoo, B. J.; Arlinghaus, H. F.; Tyler, B. J. *J. Am. Soc. Mass Spectrom.* **2023**, *34*, 218−226.
(50) Pernber, Z.; Richter, K.; Mansson, J. E.; Nygren, H. *Biochim. Biophys. Acta* **2007**, *1771*, 202−209.
(51) Yuki, D.; Sugiura, Y.; Zaima, N.; Akatsu, H.; Hashizume, Y.; Yamamoto, T.; Fujiwara, M.; Sugiyama, K.; Setou, M. *Neuroscience* **2011**, *193*, 44−53.
(52) Kollmer, F.; Paul, W.; Krehl, M.; Niehuis, E. *Surf. Interface Anal.* **2013**, *45*, 312−314.
(53) Angerer, T. B.; Blenkinsopp, P.; Fletcher, J. S. *Int. J. Mass Spectrom.* **2015**, *377*, 591−598.
(54) Shon, H. K.; Kim, S. H.; Yoon, S.; Shin, C. Y.; Lee, T. G. *Biointerphases* **2018**, *13*, No. 03B411.